Japanese Journal of Applied Physics

The Japan Society of Applied Physics

REGULAR PAPER

High-quality InP/SOI heterogeneous material integration by room temperature surface-activated bonding for hybrid photonic devices

To cite this article: Yuning Wang *et al* 2020 *Jpn. J. Appl. Phys.* **59** 052004

View the article online for updates and enhancements.

This content was downloaded from IP address 131.112.125.216 on 02/06/2020 at 12:00

https://doi.org/10.35848/1347-4065/ab8434

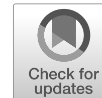

High-quality InP/SOI heterogeneous material integration by room temperature surface-activated bonding for hybrid photonic devices

Yuning Wang[1], Kumi Nagasaka[1], Takuya Mitarai[1], Yoshitaka Ohiso[1], Tomohiro Amemiya[1,2], and Nobuhiko Nishiyama[1,2*]

[1]*Department of Electrical and Electronic Engineering, Tokyo Institute of Technology, O-Okayama, Meguro, Tokyo 152-8552, Japan*
[2]*Institute of Innovative Research (IIR), Tokyo Institute of Technology, O-Okayama, Meguro, Tokyo 152-8552, Japan*

[*]E-mail: nishiyama@ee.e.titech.ac.jp

Received January 18, 2020; revised March 13, 2020; accepted March 26, 2020; published online April 23, 2020

Heterogeneous wafer bonding of InP/Si at room temperature is studied using surface-activated bonding (SAB) technology. To minimize the degradation of optical property while maintaining enough bonding strength, various bonding conditions including gas species of fast atom beam (FAB) were examined. The results show that a bonding strength of over 0.5 MPa can be obtained with less degradation of photoluminescence (PL) property of InP/Si hybrid wafer by combining Xe and Ar gases for FAB. Using this condition, hybrid wafer including quantum wells were fabricated, which showed sufficient PL property for the fabrication of hybrid photonic devices. The bonding conditions described in this study enabled realization of continuous wave (CW) operation of InP-based layers/SOI hybrid laser. © 2020 The Japan Society of Applied Physics

1. Introduction

Recently, wafer bonding technology has become attractive for hybrid III–V/Si photonic integrated circuits (PICs)[1–5] comprising active devices such as lasers and optical amplifiers. As well as known, III–V materials directly grown on an Si substrate[6] is difficult to apply into fabrication of active devices due to the lattice mismatch between III–V materials and Si.[7–9] Recently, several groups demonstrated high quality quantum dot lasers directly grown on Si substrate. However, such studies have failed to address problems such as existing buffer layers and hardly controlling particular emission wavelength, while considering integrations with photonic and electronics devices on the Si substrate.[10–12] Wafer bonding technology is the method to solve the above problems, however, conventional wafer bonding technologies, such as the hydrophilic bonding[13,14] and plasma-activated bonding (PAB),[15–17] require a high annealing temperature in order to achieve high bonding strength. In such annealing, thermal expansion stress occurs because of the difference between the thermal expansion coefficient of III–V materials and Si.[18] For instance, the thermal expansion coefficient of InP is $4.8 \times 10^{-6}\,K^{-1}$ and Si is $2.6 \times 10^{-6}\,K^{-1}$.[7] Thermal expansion stress affects optical property of the active layer such as the hybrid laser due to the generating dislocation from the interface. Further, the annealing process requires a lengthy process time because it first needs a slow temperature rise followed by a gradual temperature decrease period to reduce the influence of different thermal expansion. Therefore, lower temperature bonding, ultimately room temperature wafer bonding technology, plays a vital role in fabrication III–V/Si hybrid integration[19,20] for achieving high-quality PICs.

Surface-activated bonding (SAB) based on fast atom beam (FAB)[21–23] is one of the most popular room temperature wafer bonding technologies. Homogeneous bonding of semiconductors such as sapphire, Si, GaAs, InP, GaP, and InAs[24] and heterogeneous bonding of these materials via SAB have been reported.

As wafer bonding is conducted at room temperature in SAB, both mismatch and problem with thermal expansion coefficient difference are expected to be improved.[25] However, although there is no thermal expansion stress similar to hydrophilic bonding and PAB, crystal damage introduced by FAB irradiation may be the most important factor of optical property degradation in SAB when fabricating hybrid active devices. Therefore, it is necessary to minimize the damage introduced by FAB irradiation. Argon (Ar) is widely used for FAB irradiation. However, it was investigated that different species showed different behaviors to bonding interface.[26] Therefore, optical property is also expected to have such dependence.

In this study, we investigate the bonding quality of InP-based layers/Si, silicon-on-insulator (SOI) wafers based on SAB technology, especially for maintaining optical property of large scale PICs in telecom wavelength (1.3 μm or 1.55 μm). Firstly, the most suitable bonding condition of InP-based layers/Si wafer bonding for minimizing degradation introduced by FAB irradiation and achieving sufficient bonding strength are investigated in Sects. 2 and 3. Subsequently, wafer quality is investigated after substrate removal, including a preliminary hybrid laser fabrication and presented in Sect. 4.

2. FAB irradiation effect to photoluminescence of III–V wafers

Figure 1 schematically shows the bonding process of SAB using irradiation of FAB. A wafer's surface, covered by native oxide film or some contaminations, is irradiated and activated by inert gas radicals. The activated state of surface means that the dangling bonds of atoms exist on the surface. The exposed atoms become unstable and try to connect with other atoms, surface-activated wafers are attached to each other, and the interatomic stress works between the two substrates to form the bond. After the alignment of the irradiated wafers, two wafers are pressed in an ultra-high vacuum chamber of 10^{-6} Pa, which is a principal condition in the SAB process to maintain the wafer surface active rather than oxidized. In case of low vacuum levels, where many gaseous molecules are present, the activated surface is easily re-contaminated. Therefore, processing under ultra-high vacuum is required. Meanwhile, there is no heating process during the SAB process based on FAB. This fact contributes to having a high efficiency bonding process and reducing the defects introduced by thermal expansion stress on a bonded wafer.

For introducing SAB based on FAB irradiation into InP/Si hybrid integrated circuits, it is necessary to study the

 © 2020 The Japan Society of Applied Physics

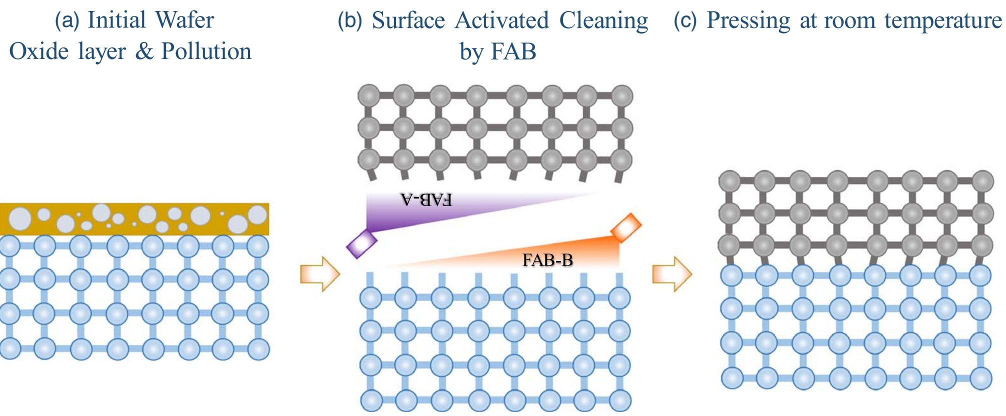

Fig. 1. (Color online) Schematic image of the bonding process of surface-activated bonding based on a fast atom beam.

dependence of the damage introduced in the semiconductor crystal on the type of gas used for FAB irradiation. In order to get insights on the most suitable gas species to the InP wafer, in this study several types of gas species are considered. Photoluminescence property has the merits as the measurement property of having a wide spectral coverage, generally nondestructive characteristic, and no special pretreatment required, thus, variation of photoluminescence (PL) property is used as the method to evaluate damage to the semiconductor crystal.[27,28]

The wafer layer structure used in this experiment is shown in Fig. 2. The sample wafer consisted of four GaInAs quantum wells (QWs) with different thicknesses (3 nm, 5 nm, 9 nm, 33 nm) at different depths (50 nm, 250 nm, 450 nm, 650 nm) respectively, separated by a 200 nm InP layer. As the four QWs have different emission wavelengths because of quantum-size effect, depth dependence of the damage introduced by FAB irradiation can be confirmed by the degradation ratio of each quantum well. In this FAB irradiation experiment, five types of FAB gas species (Xe, Kr, Ar, Ne, N_2) were evaluated.

PL intensity was measured twice, before and after FAB irradiation, to derive the amount of degradation due to the irradiation. A 1064-nm yttrium-aluminum-garnet (YAG) laser was used as the pumping light source. PL spectra of the sample wafer irradiated by Xe, Kr, Ar, Ne, N_2-FAB is shown in Figs. 3–7. In order to evaluate the degradation of the PL intensity after FAB irradiation, irradiation time dependence of the normalized PL intensity is shown in Fig. 8. The PL intensities at the 450 nm quantum well were mostly over 80% for all five types of FAB sources. Moreover, only the normalized PL intensity at 250 nm QW and 50 nm QW are shown. PL intensity decreases with increasing both FAB irradiation time and FAB current for all types of FAB sources, which means short irradiation time and low FAB current should be chosen to achieve the lowest crystal damage. However, the amount of degradation showed a source dependence. FAB source dependence on PL intensity degradation is like Ne > N_2 > Ar > Kr > Xe under the same irradiation conditions as the same as the order of atomic mass. The heavy atom has the least effect on PL intensity at both 50 and 250 nm quantum well.

Another important parameter is the FAB irradiation current dependence of PL intensity, which is corresponding to FAB irradiation energy. Figure 9 shows the dependence of PL intensity at 50, 250 and 450 nm QWs after FAB irradiation. At each QW, the normalized PL intensity decreases with increasing irradiation current for all types of FAB gas species, which means PL intensity decreases with increasing FAB irradiation energy. Among the five species, the results of Xe-FAB show the least degradation of PL intensity at all QWs. Moreover, the normalized PL intensity is kept >85% at 250 nm and 450 nm QWs with FAB irradiation current of 5 mA.

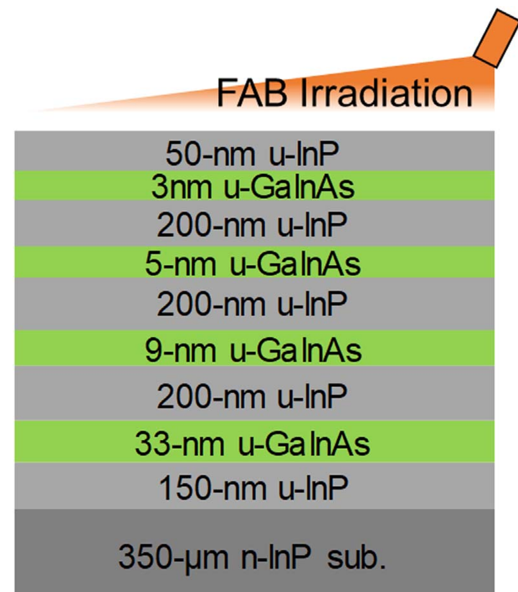

Fig. 2. (Color online) Wafer layer structure.

Based on the simulation result by Stopping and Range of Ions in Matter (SRIM) software, which is commonly used in the ion implantation simulation, the deepest penetration depth was about 10 nm when the FAB source is Ne. Simulation parameters were set to an irradiation angle of 27° that was matched to our equipment and an irradiation energy of 1 keV. Figure 10 shows the simulation results of the vacancy distribution in InP caused by Xe, Kr, Ar, Ne and demonstrates that the defect depths are like Ne > Ar > Kr > Xe, which is the same as atomic mass order. The heavier atom forms the shallower defect depth in the InP semiconductor crystal, which agrees with the PL intensity degradation after FAB irradiation. We also obtained a transmission electron

 © 2020 The Japan Society of Applied Physics

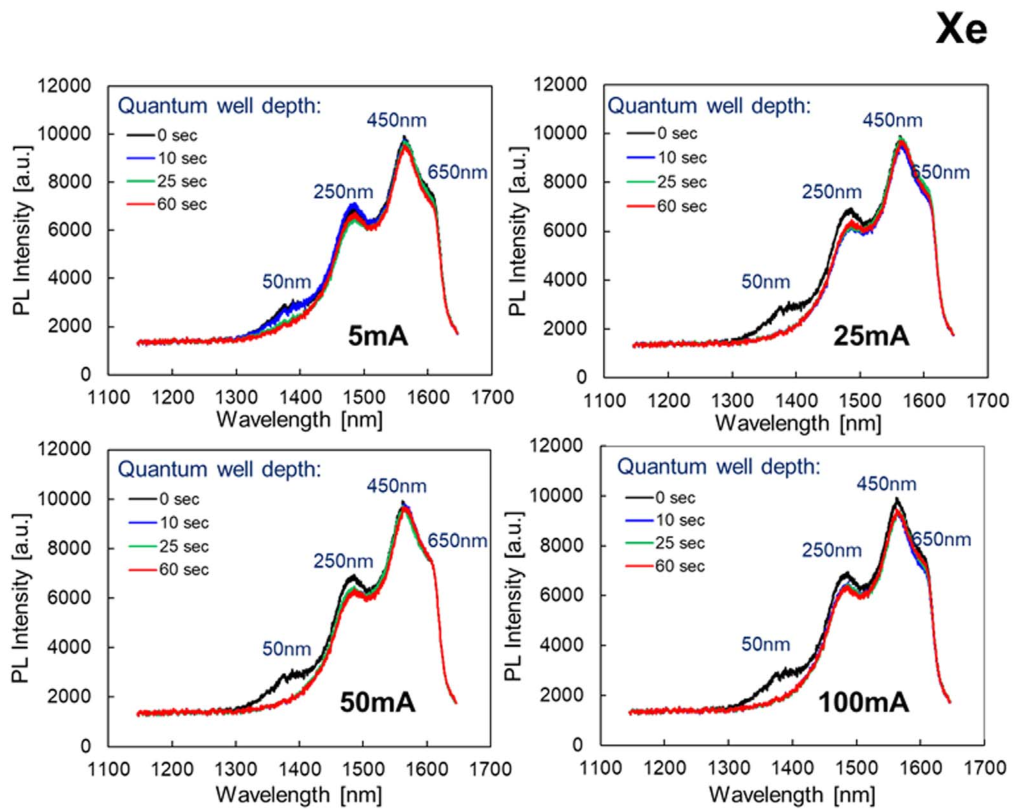

Fig. 3. (Color online) PL spectra for Xe-FAB currents of (a) 5 mA, (b) 25 mA, (c) 50 mA, and (d) 100 mA (excitation wavelength: 1064 nm).

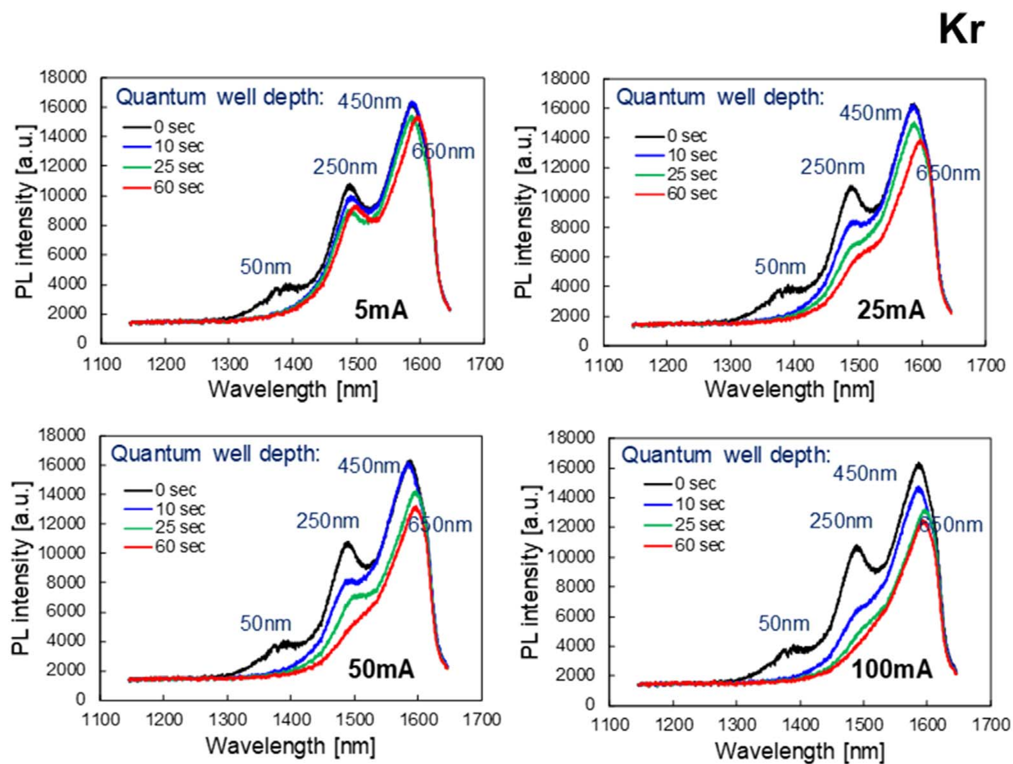

Fig. 4. (Color online) PL spectra for Kr-FAB currents of (a) 5 mA, (b) 25 mA, (c) 50 mA, and (d) 100 mA (excitation wavelength: 1064 nm).

microscope (TEM) cross section image of the bonded III–V/Si wafers, which will be described in detail in the following section. There is an amorphous layer between III–V and the Si wafer, and the thickness of the amorphous layer agreed with the simulation result of the vacancy distribution in InP.

Interestingly, the depth in the simulation was different from what we observed in PL intensity degradation. Therefore, the reason for PL intensity degradation is not directly related to the defect caused by atom penetration. A possible explanation for this might be due to the defect

 © 2020 The Japan Society of Applied Physics

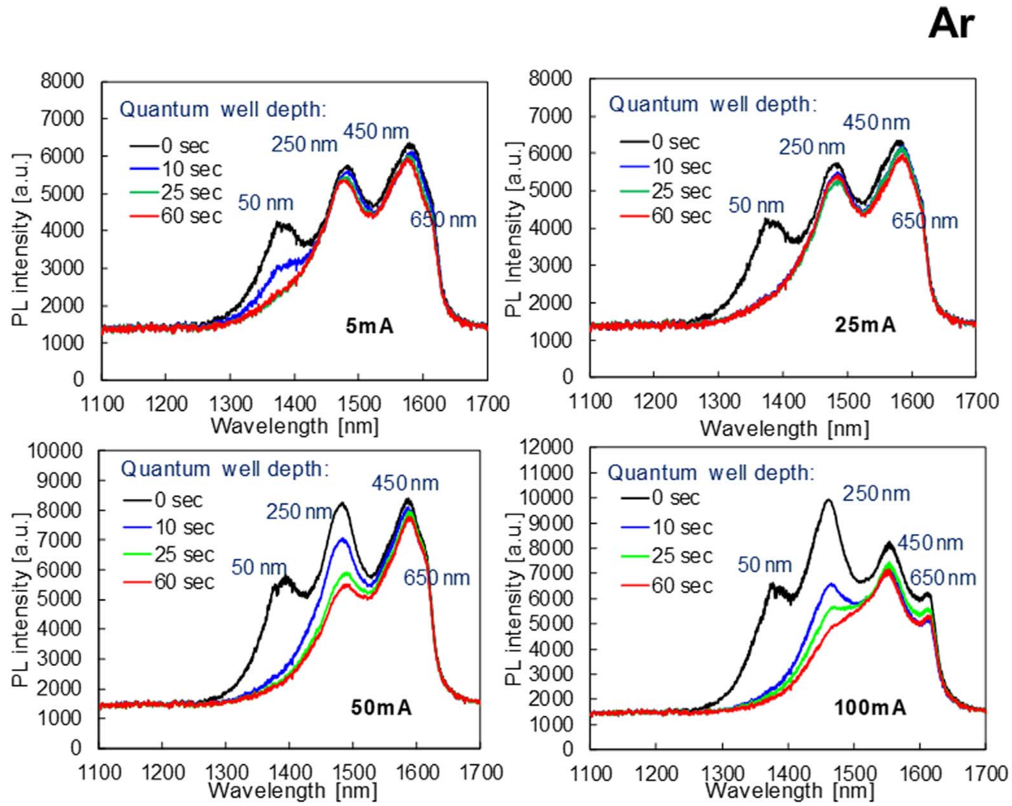

Fig. 5. (Color online) PL spectra for Ar-FAB currents of (a) 5 mA, (b) 25 mA, (c) 50 mA, and (d) 100 mA (excitation wavelength: 1064 nm).

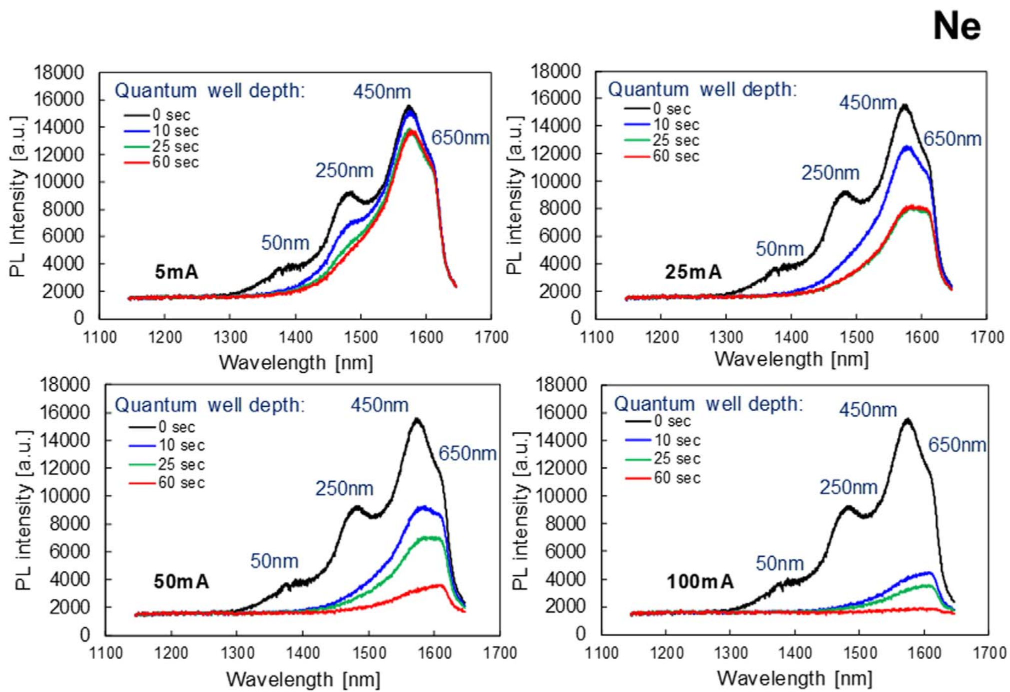

Fig. 6. (Color online) PL spectra for Ne-FAB currents of (a) 5 mA, (b) 25 mA, (c) 50 mA, and (d) 100 mA (excitation wavelength: 1064 nm).

caused by the propagation of energy through phonon or creation of the carrier trap at the surface to enhance non-radiative recombination. Actually, we can observe the amorphous-like layer at the surface, which will be explained in Sect. 4. This thickness could be related to the PL intensity degradation. Less FAB irradiation energy contributes to less of an amorphous layer and less PL intensity degradation.[29] Although we have no direct evidence at this moment, the amorphous layer might increase non-radiative recombination.

As a conclusion, Xe-FAB has the least effect on PL intensity under the same FAB irradiation conditions, which

 © 2020 The Japan Society of Applied Physics

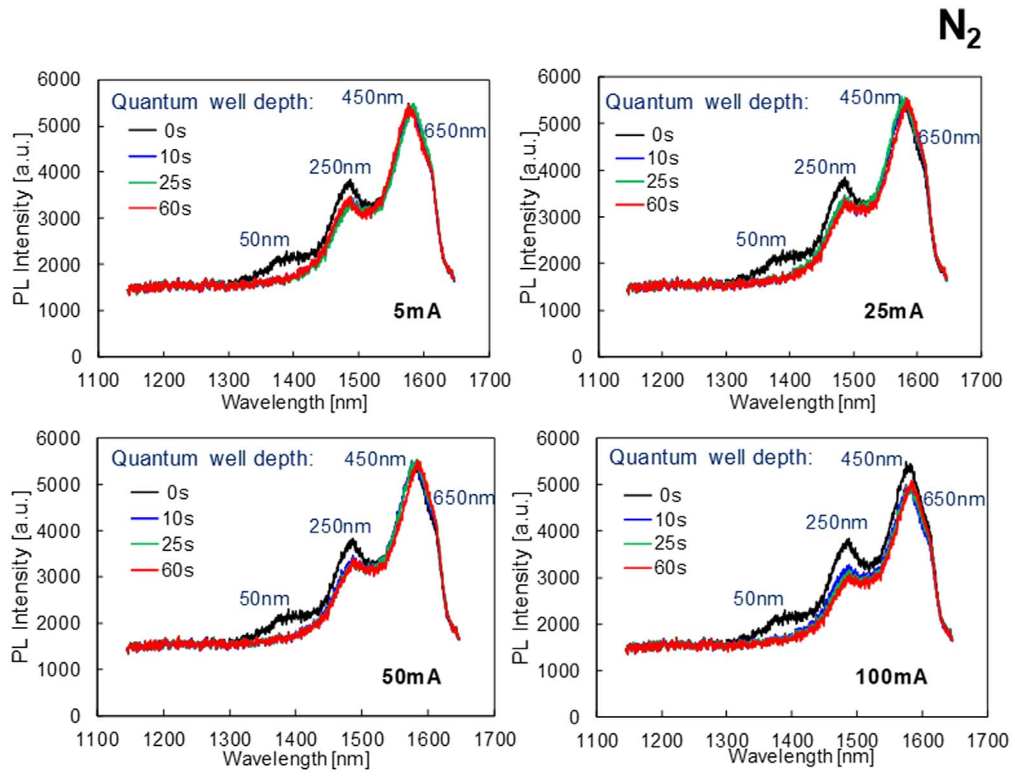

Fig. 7. (Color online) PL spectra for N_2-FAB currents of (a) 5 mA, (b) 25 mA, (c) 50 mA, and (d) 100 mA (excitation wavelength: 1064 nm).

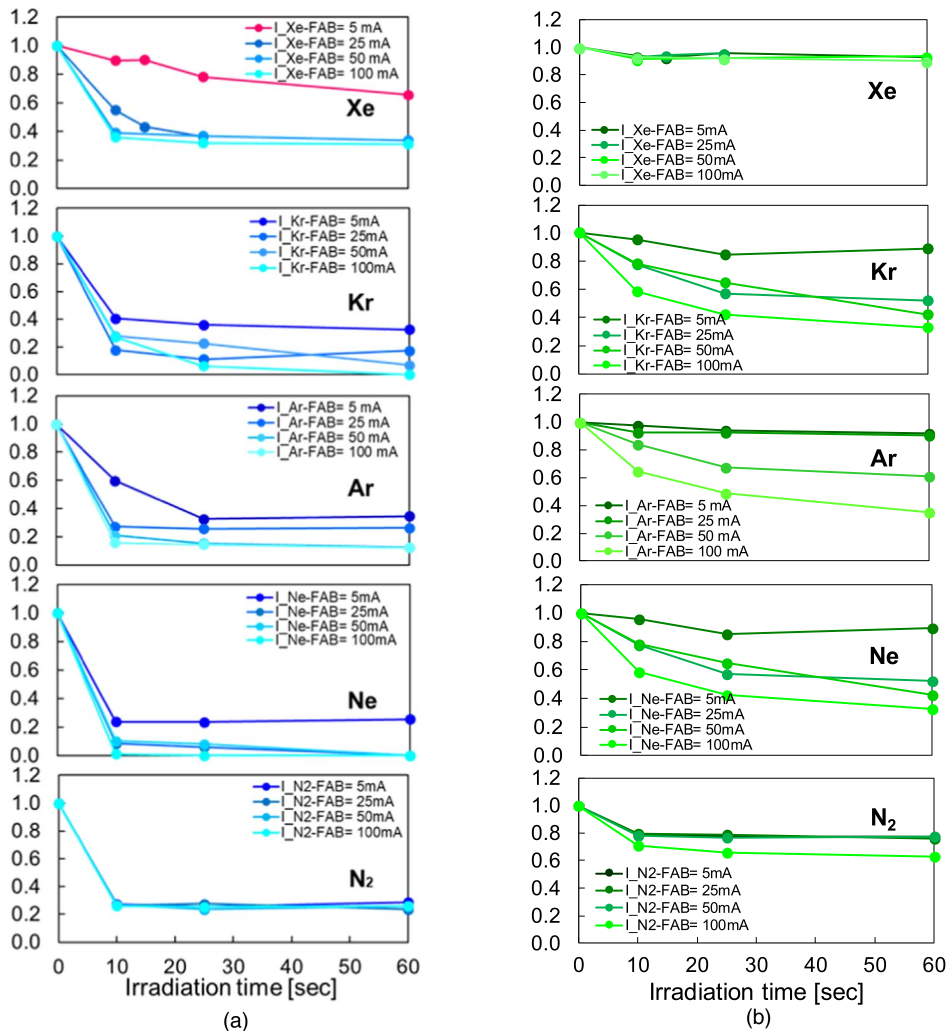

Fig. 8. (Color online) Irradiation time dependence of the normalized PL intensity at (a) 50 nm and (b) 250 nm quantum well depth.

© 2020 The Japan Society of Applied Physics

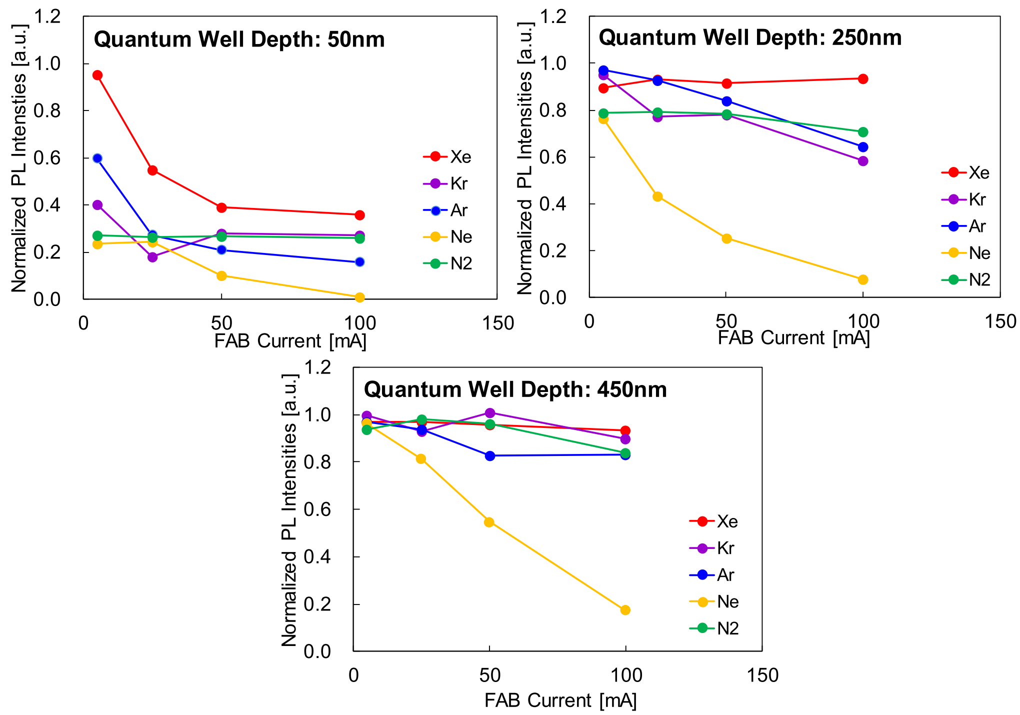

Fig. 9. (Color online) Irradiation current dependence of the normalized PL intensity (FAB irradiation time: 10 s).

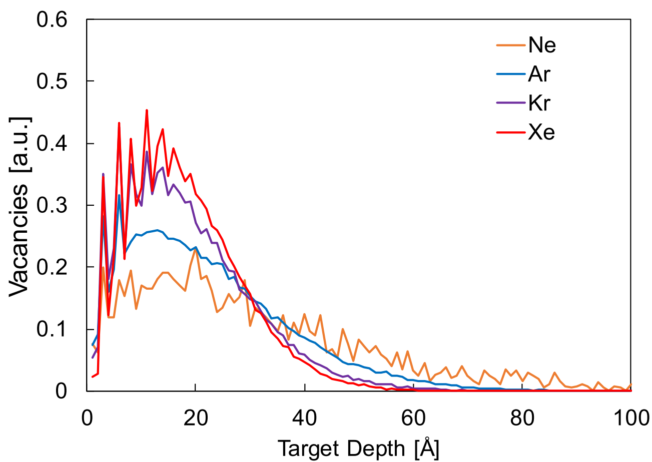

Fig. 10. (Color online) Vacancy distribution dependence on target depth (target: InP, irradiation energy: 1 keV, irradiation angle: 27°).

means Xe-FAB should be chosen as the FAB source for the InP wafer.

3. InP/Si wafer bonding process based on Xe & Ar-FAB

As mentioned before, a wafer sample irradiated by Xe-FAB has the least effect on PL intensity. To introduce this Xe-FAB irradiation condition into InP/Si wafer bonding for maintaining optical property of the hybrid optical device, it is necessary to study the InP/Si wafer bonding condition as the initial step. However, InP/Si wafer bonding cannot be achieved by Xe-FAB according to our trial experiment results. Due to the atomic radius of Xe being relatively bigger compared with other inert gas atoms, the roughness of wafer surface irradiated by Xe is bigger than the sample irradiated by other inert gases.[30]

Therefore, to achieve enough bonding strength and improved optical property, InP/Si wafer bonding using two gases, Xe and Ar, was carried out. To maintain the PL intensity after FAB irradiation, Xe was selected to be the FAB source of the InP wafer. Moreover, for achieving enough bonding strength, Ar was selected to be the FAB source of the Si wafer, which is commonly used for Si bonding. This means FAB-A is Xe and FAB-B is Ar in Fig. 1.

Before the wafer bonding process, a wet chemical cleaning process was performed to remove both native oxide and contamination. After the wafer cleaning process, both the Si wafer and InP wafer were put in the chamber of the SAB system. The Si and InP wafers were fixed to the chamber's upper and lower side. Subsequently, FAB irradiation was carried out by two FAB guns with different gases from the irradiation angle of 27°. After irradiation, InP and Si wafers were pressed at 2 MPa under 25 °C in an ultra-high-vacuum chamber.

Comparison of bonding strength under various irradiation conditions of Xe to InP wafers was performed. The FAB irradiation conditions of Si and InP wafer are shown in Tables I and II. The irradiation condition of Si was fixed according to Si/Si bonding strength in our prior experiments.

Based on the results described in the previous section, the PL intensity presents an insignificant degradation when quantum well depth is deeper than 50 nm. Therefore, to get insights on the suitable irradiation condition of the InP wafer,

Table I. FAB irradiation condition of Si in the bonding experiment.

Wafer	Gas	Gas Flow	Irradiation current	Irradiation voltage	Irradiation time
Si	Ar	30 sccm	50 mA	1.07 kV	90 s

© 2020 The Japan Society of Applied Physics

Table II. FAB irradiation condition of InP wafer in bonding experiment.

Wafer	Gas	Gas Flow	Irradiation current	Irradiation voltage	Irradiation time	Bonding strength
InP	Xe	17 sccm	25 mA	1.06 kV	10 s	0.48 MPa
		17 sccm	35 mA	1.03 kV		0.58 MPa
		20 sccm	50 mA	1.04 kV		0.39 MPa
	Ar	30 sccm	25 mA	0.90 kV	10 s	0.91 MPa
			50 mA	1.10 kV		2.05 MPa
			100 mA	1.33 kV		1.76 MPa

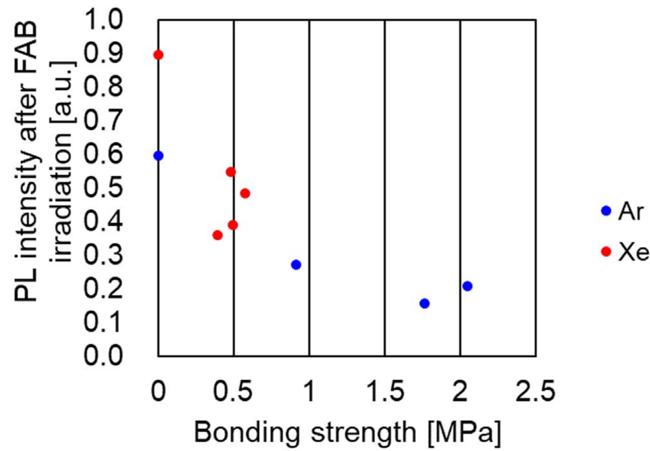

Fig. 11. (Color online) Relation between PL intensity after FAB irradiation of 50 nm quantum well and bonding strength.

a relation between the PL intensity of 50 nm QW after FAB irradiation and the bonding strength is shown in Fig. 11. The bonding strength was measured by the pulling test of bonded 2-inch wafers. Although the maximum bonding strength of the wafer bonded using Ar-FAB (current: 50 mA) is over 2 MPa, which is stronger than the maximum bonding strength of the wafer bonded using Xe-FAB (current: 35 mA), the PL intensity after FAB irradiation drastically decreased when the FAB source of InP wafer is Ar. At the bonding strength of 0.5 MPa, the PL intensities are kept over 50% for Xe and 40% for Ar at 50 nm quantum well depth. In our previous research, we found that a bonding strength of 0.5 MPa is good enough to process hybrid photonic devices.[31] Therefore, Xe-FAB could be the better choice for achieving enough bonding strength for hybrid laser process as well as for keeping PL intensity after FAB irradiation. Please note the depth position of the active layers for actual hybrid photonic devices are deeper than several hundred nm. Thus, the PL intensity in real devices can be maintained as high as over 85% according to Fig. 8.

4. Evaluation of bonding quality after removal of InP substrate

Finally, we evaluated the bonding quality after removing the InP host substrate. Figure 12(a) shows the layer structure of the InP epitaxial wafer on the Si substrate after the removal of the InP substrate. This epitaxial wafer consists of an active layer of GaInAsP five quantum wells (5QWs), emitting at 1550 nm, sandwiched by InP cladding layers, and superlattice layer consisting of 14 pairs of 7 nm-GaInAsP and 6 nm-InP which is an interlayer for blocking various dislocations generated from the interface caused by the wafer bonding process.[32]

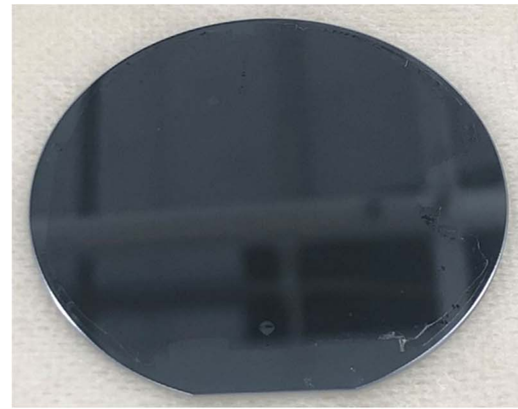

(a)

(b)

Fig. 12. (Color online) Image of (a) InP-based layers/Si wafer after the InP substrate and GaInAs etching stop layer removal and (b) layer structure of InP-based layers/Si wafer after InP substrate and GaInAs etching stop layer removal.

After InP-based layers/Si wafer bonding process mentioned in the previous section, the hybrid wafer was polished to 100 μm and subsequently dipped in HCl solution at a temperature of 40 °C for the removal of the InP substrate up to an etching stop layer. To achieve the accurate comparison, the GaInAs etching stop layer ($\lambda_g \sim 1.65$ nm) was also removed by H_2SO_4:H_2O_2:H_2O solution (1:1:40) under the temperature of 25 °C. The surface image of the wafer after substrate removal is shown in Fig. 12(b). There are no obvious voids and just a little bit peeling off at orientation flat and the right side of wafer due to held by tweezers during the wafer bonding process.

Figure 13 shows PL mapping images of (a) the initial InP-based epitaxial wafer, (b) InP-based layers/Si wafer after the InP substrate and GaInAs etching stop layer removal, and (c)

 © 2020 The Japan Society of Applied Physics

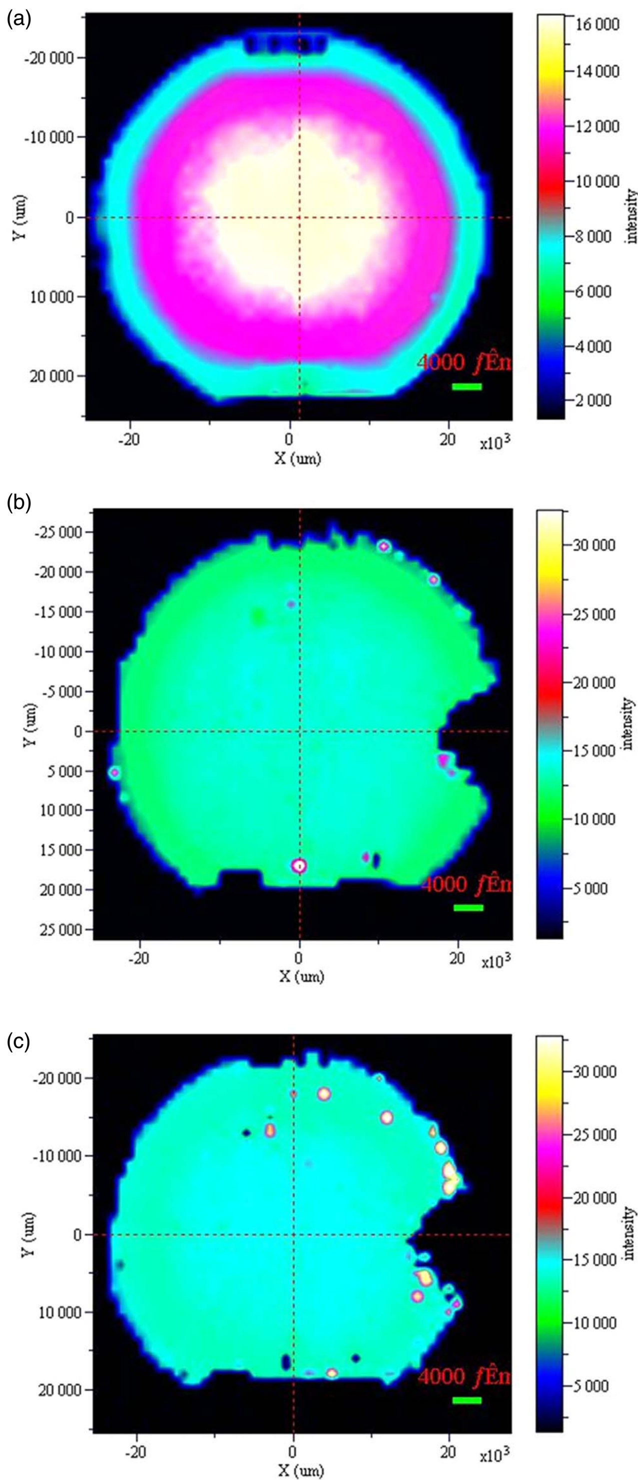

Fig. 13. (Color online) PL mapping image of (a) as-grown InP-based epitaxial wafer before bonding, (b) InP-based layers/Si wafer after bonding and (c) InP-based layers/Si wafer after 280 °C.

InP-based layers/Si wafer after heating at 280 °C. The heating process was set to be 280 °C because the process temperature of SiO_2 deposition process in hybrid laser fabrication process is at about 280 °C.

From the PL mapping images, there is a uniform epitaxial layer bonded on the Si wafer. The PL mapping image after 280 °C heating is almost the same with the one before heating.

Figure 14 shows (a) PL spectra of the center point of bonded InP/Si wafer (b) wavelength peaks in three PL spectra. There is barely no degradation of PL intensity and variation of PL spectrum shape even after bonding and heating at 280 °C. About the wavelength shift after wafer bonding process and heating at 280 °C, a blue shift of 6.8 nm is present. There were no differences between the wafer after the bonding process and wafer after heating process at 280 °C (initial InP epitaxial wafer: 1553.6 nm, after removal of InP substrate: 1546.8 nm, after heating at 280 °C: 1546.8 nm).

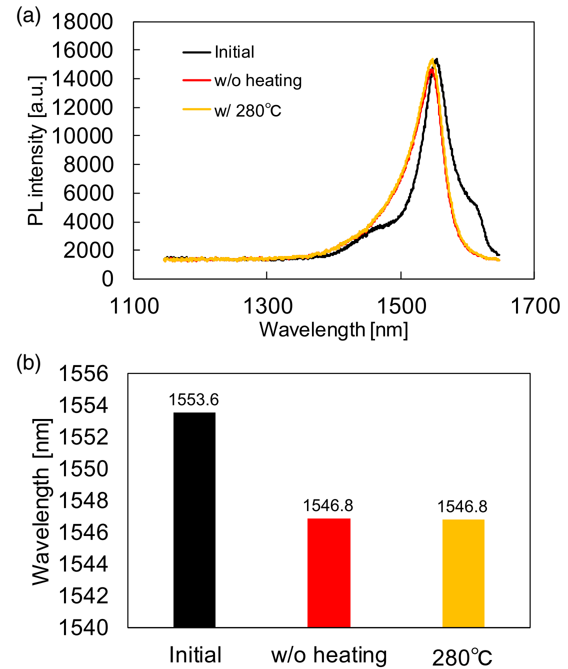

Fig. 14. (Color online) (a) PL spectra of center point of epitaxial wafer before bonding, InP/Si wafer without heating, and InP/Si wafer after 280 °C, and (b) wavelength shift of main peak in three PL spectra.

Figure 15 shows the TEM cross-sectional image of (a) complete structure (b) wafer bonding interface of the hybrid wafer. As shown in the figures, the 5QWs structure remains after wafer bonding and the heating process at 280 °C. There is an amorphous-like intermediate layer with the thickness of 3 nm between the InP-based epitaxial layers and Si wafers.[33] Comparing with the other kinds of FAB gas species, such as Ne, Ar, the sample bonded by Xe-FAB has a relatively thinner amorphous layer,[25,29] corresponding to the less degradation of PL intensity. To investigate the variation of the peak wavelength, the XRD scan data of as-grown InP-based layers and bonded InP-based layers/Si were measured in Fig. 16. The result of calculated fitting curves reveals that the compressive strain of well layers slightly reduced from 0.98% to 0.975%.

Because PL wavelength depends on the strain in MQWs sensitively, we assumed that the reason why 6.8 nm blue-shift of wavelength in the PL spectrum after wafer bonding process is compressive strain relaxation in the MQWs layer caused by the removal of the InP substrate and GaInAs etching stop layer. It is assumed that strain relaxation resulted in the level of heavy hole in the valence band of quantum well dropping.

As the thermal expansion coefficients are different between InP and Si, the thermal expansion mismatch between InP and Si contributes to form the peak wavelength shift after the wafer bonding process for conventional wafer bonding

 © 2020 The Japan Society of Applied Physics

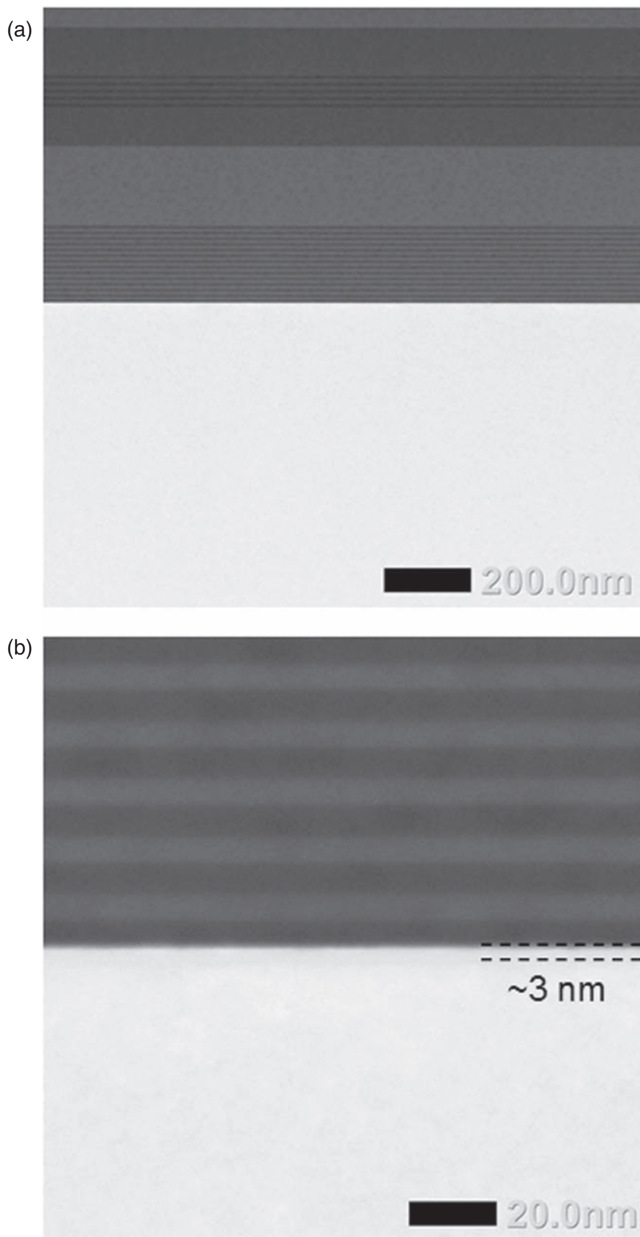

Fig. 15. (Color online) TEM image of (a) bonded InP-based layers/Si wafer and (b) wafer bonding interface.

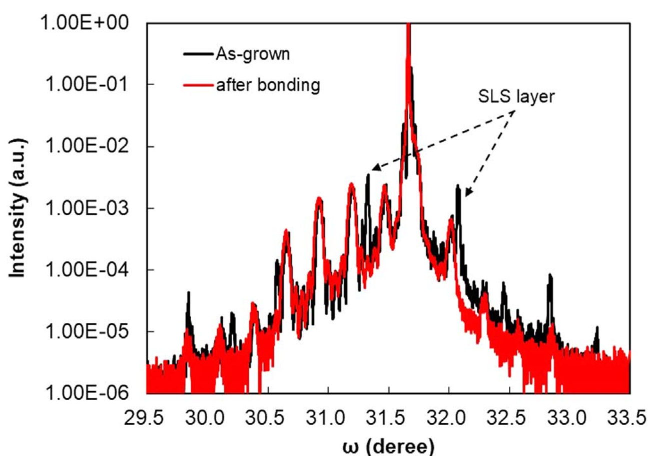

Fig. 16. (Color online) High-resolution XRD measurement of as-grown InP-based wafer and after bonding wafer.

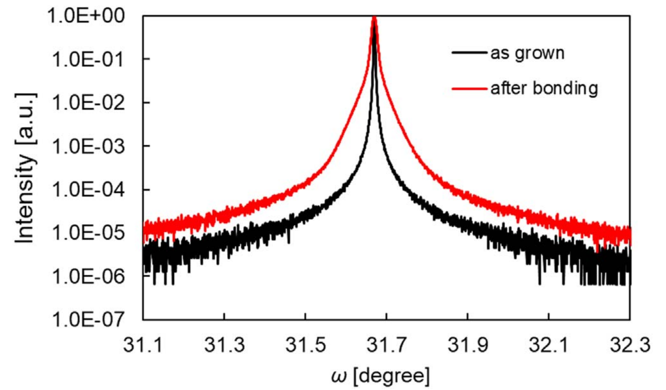

Fig. 17. (Color online) High-resolution omega scans of InP peak in XRD measurement of as grown epitaxial wafer and InP-based layers/Si wafer after bonding.

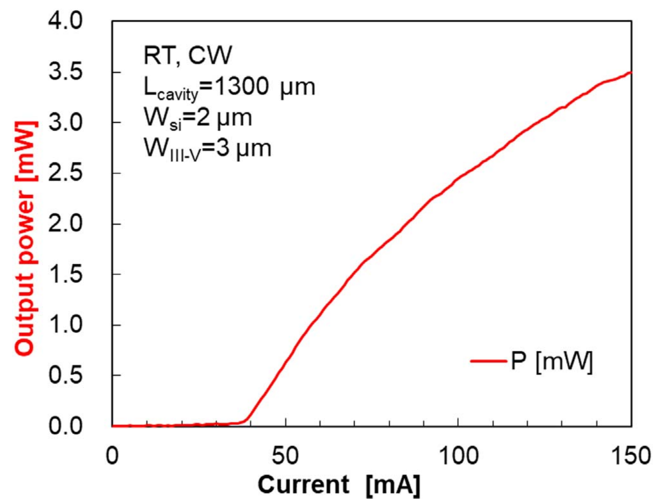

Fig. 18. (Color online) I-L characteristics of hybrid InP-based layers/SOI FP laser.

technologies. However, in this work, there is no PL wavelength shift after heating at 280 °C, which means that thermal expansion takes place independently at Si and InP owing to the amorphous layer, which is a buffer layer at the bonding interface between III–V and Si wafer.

To evaluate the bonding quality of InP-based layers/Si wafer from another point of view, we also measured high-resolution omega scans of InP peak of as-grown epitaxial wafer and InP-based layers/Si wafer after bonding by X-ray diffraction (XRD) as shown in Fig. 17. A FWHM of the InP peak is 12.24″, which is attributed to a grown InP-based epitaxial wafer. Moreover, the FWHM of the InP peak is 45.57″, which is attributed to InP-based layers/Si wafer. This result demonstrates that even the strain generated at the bonding interface is relatively small, which contributes to barely no degradation of the PL intensity at MQWs by the bonding itself.

This result also shows that SAB based on Xe & Ar-FAB at room temperature is suitable to be introduced in the fabrication of high-quality III–V/Si hybrid laser.

Using this developed technology, we then fabricated a hybrid InP-based layers/SOI Fabry–Pérot (FP) laser. The wafer structure was similar to the structure shown in Fig. 12; however, the SOI wafer had waveguide patterns. Current-light (I-L) characteristics under 20 °C continuous wave

 © 2020 The Japan Society of Applied Physics

operation is shown in Fig. 18. The laser operation was achieved using SAB at room temperature. The threshold current and output power of this hybrid FP laser is 35 mA and over 3 mW with a 1300 μm-cavity-length corresponding to a reasonable threshold current density of 897 A cm^{-2}. This result indicates that the bonding condition described in the previous sections is suitable for the fabrication of a hybrid laser.

5. Conclusion

In this work, we investigated SAB at room temperature to achieve both enough bonding strength and optical property for hybrid photonic devices based on heterogeneous integration. To suppress the degradation of PL intensity by FAB irradiation, five types of FAB gas species were evaluated for irradiation. We found out that among the five types of gas species, Xe-FAB is the suitable choice. The bonding condition that could be introduced into the hybrid laser fabrication process is the InP epitaxial wafer: 35 mA 10 s by Xe-FAB and Si wafer: 50 mA 90 s by Ar-FAB at room temperature. This condition showed a bonding strength of over 0.5 MPa and no significant PL degradation with respect to the required temperature of the fabrication process. Finally, we have fabricated a hybrid InP-based layer/SOI FP laser based on the developed bonding condition with the threshold current of 35 mA, corresponding to the threshold current density of 897 A cm^{-2}, which means SAB technology could be introduced in hybrid III–V/Si laser fabrication.

Acknowledgments

The authors would like to thank Drs. Hideki Yagi, Naoki Fujiwara, Takuo Hiratani, Mr. Toshiyuki Nitta and Takehiko Kikuchi of Sumitomo Electric Industries for their experimental help and discussions. Also, the authors would like to thank Prof. Tadatomo Suga of the University of Tokyo and Dr. Masahisa Fujino of AIST for their discussions. This work was supported by NEDO, JST-ACCEL (JPMJAC1603), JST-CREST (JPMJCR15N16), JSPS KAKENHI, grant numbers (#16H06082, #17H03247).

1) S. E. Miller, Bell Syst. Tech. J. **48**, 2059 (1969).
2) I. P. Kaminow, J. Light. Technol. **26**, 994 (2008).
3) G. Roelkens, L. Liu, D. Liang, R. Jones, A. Fang, B. Koch, and J. Bower, Laser Photonics Rev. **4**, 751 (2010).
4) T. Shimizu, N. Hatori, M. Okano, M. Ishizaka, Y. Urino, T. Yamamoto, M. Mori, T. Nakamura, and Y. Arakawa, Photonics Res. **2**, A19 (2014).
5) J. E. Bowers and A. Y. Liu, Optical Fiber Communication Conf., OSA Technical Digest, 2017 M2B.4.
6) Z. Mi and Y. L. Chang, J. Nanophotonics **3**, 031602 (2009).
7) S. F. Fang, K. Adomi, S. Iyer, H. Morkoc, H. Zabel, C. Choi, and N. Otsuka, J. Appl. Phys. **68**, R31 (1990).
8) T. Mårtensson, C. P. T. Svensson, B. A. Wacaser, M. W. Larsson, W. Seifert, K. Deppert, A. Gustafsson, L. R. Wallenberg, and L. Samuelson, Nano Lett. **4**, 1987 (2004).
9) A. Beyer, J. Ohlmann, S. Liebich, H. Heim, G. Witte, W. Stolz, and K. Volz, J. Appl. Phys. **111**, 0835341 (2012).
10) S. Chen et al., Nat. Photonics **10**, 307 (2016).
11) B. Shi, S. Zhu, Q. Li, C. W. Tang, Y. Wan, E. L. Hu, and K. M. Lau, Appl. Phys. Lett. **10**, 121109 (2017).
12) A. Y. Liu, J. Peters, X. Huang, D. Jung, J. Norman, M. L. Lee, A. C. Gossard, and J. E. Bowers, Opt. Lett. **42**, 338 (2017).
13) C. Ventosa, F. Rieutord, L. Libralesso, C. Morales, F. Fournel, and H. Moriceau, J. Appl. Phys. **104**, 1235241 (2008).
14) Y. Okuno, K. Uomi, M. Aoki, and T. Tsuchiya, IEEE J. Quantum Electron. **33**, 959 (1997).
15) D. Pasquariello, M. Camacho, K. Hjort, L. Dozsa, and B. Szentpali, Mater. Sci. Eng. B Solid **80**, 134 (2001).
16) M. M. R. Howlader, T. Suga, H. Itoh, T. H. Lee, and M. J. Kim, J. Electrochem. Soc. **156**, H846 (2009).
17) T. Plach, K. Hingerl, S. Tollabimazraehno, G. Hesser, V. Dragoi, and M. Wimplinger, J. Appl. Phys. **113**, 0949051 (2013).
18) Y. T. Sun, K. Baskar, and S. Lourdudoss, J. Appl. Phys. **94**, 2746 (2003).
19) K. Tanabe, K. Watanabe, and Y. Arakawa, Sci. Rep. **2**, 349 (2012).
20) G. H. Duan et al., IEEE J. Sel. Top. Quantum Electron. **20**, 158 (2014).
21) T. Suga, K. Miyazawa, and Y. Yamagata, Mater. Res. Soc. **8**, 257 (1989).
22) H. Takagi, K. Kikuchi, R. Maeda, T. R. Chung, and T. Suga, Appl. Phys. Lett. **68**, 2222 (1996).
23) T. R. Chung, N. Hosoda, T. Suga, and H. Takagi, Appl. Phys. Lett. **72**, 1565 (1999).
24) T. R. Chung, L. Yang, N. Hosoda, H. Takagi, and T. Suga, Appl. Surf. Sci. **117**, 808 (1997).
25) G. Kono, M. Fujino, D. Yamashita, K. Watanabe, T. Sugiyama, Y. Nakano, and T. Suga, IEEE Int. Conf. Electron. Packaging iMAPS All Asia Conf., 2015, p. 478.
26) M. Fujino, G. Kono, and T. Suga, Int. Conf. Solid State Devices Mater., 2017, p. 391.
27) S. Tongay et al., Sci. Rep. **3**, 2657 (2013).
28) W. S. Yoo, T. Ishigaki, and K. Kang, ECS J. Solid State Sci. Technol. **5**, P3064 (2015).
29) E. Higurashi et al., Jpn. J. Appl. Phys. **54**, 030213 (2015).
30) Y. Kurashima, A. Maeda, and H. Takagi, Appl. Phys. Lett. **102**, 251605 (2013).
31) Y. Hayashi et al., Jpn. J. Appl. Phys. **52**, 060202 (2013).
32) K. A. Black, P. Abraham, A. Karim, J. E. Bowers, and E. L. Hu, Int. Conf. Indium Phosphide Rel. Mater., 1999, p. 357.
33) H. Takagi, R. Maeda, T. R. Chung, N. Hosoda, and T. Suga, Jpn. J. Appl. Phys. **38**, 1589 (1999).

© 2020 The Japan Society of Applied Physics